Novel Striatal GABAergic Interneuron Populations Labeled in the 5HT3a^EGFP Mouse

A.B. Muñoz-Manchado[1,†], C. Foldi[1,†], S. Szydlowski[2,†], L. Sjulson[3,4], M. Farries[5], C. Wilson[5], G. Silberberg[2] and J. Hjerling-Leffler[1]

[1]Department of Medical Biochemistry and Biophysics, [2]Department of Neuroscience, Karolinska Institutet, Stockholm, Sweden, [3]Department of Psychiatry, [4]Department of Neuroscience and Physiology, NYU Neuroscience Institute, NYU Langone Medical Center, New York, NY, USA and [5]Department of Biology, University of Texas at San Antonio, San Antonio, TX, USA

Address correspondence to Jens Hjerling-Leffler, Department of Medical Biochemistry and Biophysics, Karolinska Institutet, Scheelesv 1, 17177 Stockholm, Sweden. Email: jens.hjerling-leffler@ki.se

[†]A. B. Muñoz-Manchado, C. Foldi, and S. Szydlowski contributed equally to this study.

Histological and morphological studies indicate that approximately 5% of striatal neurons are cholinergic or γ-aminobutyric acidergic (GABAergic) interneurons (gINs). However, the number of striatal neurons expressing known interneuron markers is too small to account for the entire interneuron population. We therefore studied the serotonin (5HT) receptor 3a-enhanced green fluorescent protein (5HT3a^EGFP) mouse, in which we found that a large number of striatal gINs are labeled. Roughly 20% of 5HT3a^EGFP-positive cells co-express parvalbumin and exhibit fast-spiking (FS) electrophysiological properties. However, the majority of labeled neurons do not overlap with known molecular interneuron markers. Intrinsic electrical properties reveal at least 2 distinct novel subtypes: a late-spiking (LS) neuropeptide-Y (NPY)-negative neurogliaform (NGF) interneuron, and a large heterogeneous population with several features resembling low-threshold-spiking (LTS) interneurons that do not express somatostatin, NPY, or neuronal nitric oxide synthase. Although the 5HT3a^EGFP NGF and LTS-like interneurons have electrophysiological properties similar to previously described populations, they are pharmacologically distinct. In direct contrast to previously described NPY^+ LTS and NGF cells, LTS-like 5HT3a^EGFP cells show robust responses to nicotine administration, while the 5HT3a^EGFP NGF cell type shows little or no response. By constructing a molecular map of the overlap between these novel populations and existing interneuron populations, we are able to reconcile the morphological and molecular estimates of striatal interneuron numbers.

Keywords: 5HT3a, interneuron, nicotine, striatum, subtype

Introduction

The striatum is comprised of a large majority of projection neurons (medium-sized spiny neurons, MSNs), and a small, yet diverse minority of interneurons, most of which are inhibitory γ-aminobutyric acidergic (GABAergic) interneurons (gINs; Kawaguchi et al. 1995). Efforts to quantify and characterize striatal interneuron diversity began with anatomical studies assessing the relative contribution of the gIN population. Since striatal gINs express higher levels of the GABA-producing enzyme Gad67 compared with MSNs (Kita 1993), earlier studies have used high Gad67 expression to determine the relative contribution of the gINs to be 4–8% of neurons in the striatum (Kita and Kitai 1988; Lindefors et al. 1989). The gINs also have a higher uptake of surrounding GABA, and by injecting tritiated GABA into the striatum it was shown that gINs have a nuclear envelope with characteristic indentations (Iversen and Schon 1973; Bolam et al. 1983) that are also found in aspiny choline acetyltransferase (ChAT)-expressing cholinergic interneurons (Phelps et al. 1985). Prior anatomical work based on these nuclear indentations has estimated the interneuron

population in the rodent striatum to constitute approximately 5% of all neurons (Graveland and DiFiglia 1985).

Telencephalic gINs are highly heterogeneous, but major groups can be distinguished based on the expression of histochemical markers. In the rodent striatum, parvalbumin (PV)-expressing cells are FS (with short half-width action potentials, APs) basket cells, whereas the somatostatin (SST)-expressing cells are low-threshold-spiking (LTS) cells with an extended axonal arborization. Most SST cells also express neuropeptide-Y (NPY) and neuronal nitric oxide synthase (nNOS; Vuillet et al. 1990). A third group of interneurons expresses calretinin (CR), although there seem to be a clear species difference with far fewer CR cells observed in the mouse when compared with the rat. This list of gIN subtypes has recently been expanded with a number of new subtypes, including an NPY-expressing (SST-negative) neurogliaform (NGF) cell and a heterogeneous group expressing tyrosine hydroxylase (TH; Ibanez-Sandoval et al. 2010, 2011; Tepper et al. 2010).

The 2 largest subpopulations are PV- and SST-expressing, and their relative contributions to striatal neuronal numbers are approximately 0.5% and 0.8%, respectively (Oorschot 2013). Taken together, the number of cells belonging to the molecularly defined classes of interneurons in the striatum accounts for a total of 2.2–3.7% (cholinergic interneurons: 0.4–1.5% and gINs: 1.8–2.2%; Gerfen and Wilson 1996; Luk and Sadikot 2001; Rymar et al. 2004; Tepper et al. 2010). In recent years, a number of genetic strategies to target striatal interneuron populations have been developed that do not rely on the aforementioned markers, but rather on genetic programs necessary for development or indicative of their developmental origin. However, these mouse lines either (1) label only cells derived from the medial ganglionic eminence (MGE) and preoptic area (POA): the PV-, SST-, CR-, and/or ChAT-expressing cells (Lhx6^cre/egfp, Nkx2-1^cre), or (2) also label a significant number of MSNs derived from the lateral ganglionic eminence (LGE; Dlx1/2^CreER, Dlx1-venus^fl, Gad1^cre/egfp). This has so far precluded an overarching analysis of interneuron numbers (Xu et al. 2008; Fragkouli et al. 2009; Gittis et al. 2010; Rubin et al. 2010).

In the mouse cortex, nearly all gINs fall into 1 of 3 non-overlapping populations that express PV, SST, or the ionotropic serotonin (5HT) receptor subunit 3a (5HT3a) (Lee et al. 2010; Rudy et al. 2011). The 5HT3a-expressing neurons are derived from the caudal ganglionic eminence (CGE) and respond robustly to activation of nicotinic acetylcholine receptors (nAChRs). In the striatum, there is evidence for nAChR-dependent GABAergic signaling that so far cannot be mapped onto any of the known MGE-derived subtypes (Sullivan et al. 2008), suggesting that there remain undescribed gIN subtypes in the striatum.

In this study, we describe 2 novel subpopulations of striatal gINs labeled in the 5HT3a^EGFP mouse line. These subpopulations

are molecularly and pharmacologically distinct from previously described subtypes. Furthermore, by constructing a comprehensive map of the relative contributions and overlap of molecularly defined dorsal striatal interneuron populations, we show that the addition of these 2 subpopulations nearly doubles the relative size of the identified gIN population, to match the 5% estimated by morphological and histological studies.

Materials and Methods

Transgenic Mice

We used the transgenic mouse 5HT3a[EGFP] on a CD-1 background to characterize the EGFP-expressing cells in striatum. In this mouse line, EGFP is expressed under the control of the *Htr3a* promoter (GENSAT project, Rockefeller University, NY, USA). To construct the striatal interneuron map we also utilized the wild-type CD-1 mouse strain. For nicotine response recordings we used Lhx6[EGFP] mice as controls (GENSAT project). We used the *B6.FVB-Tg (NPY-hrGFP)1Lowl/J* strain (Jackson Laboratory, CA, USA) mouse to confirm our immunostainings for NPY. Experimental animals included mice of both sexes. All experimental procedures performed on animals following the guidelines and recommendations of local animal protection legislation and were approved by the local committees for ethical experiments on laboratory animals (Stockholms Norra Djurförsöketiska nämnd, Sweden, and The University of Texas at San Antonio IACUC).

Tissue Preparation for Immunofluorescence and In Situ Hybridization

Brains from P21–P28 5HT3a[EGFP] or wild-type mice were dissected after transcardiac perfusion with 10 mL of phosphate-buffered saline (PBS) and 25 mL of 4% paraformaldehyde (PFA) in PBS consecutively, followed by 1 or 4 h (immuno and in situ, respectively) postfixation with 4% PFA at 4 °C. Tissue was cryoprotected using a 15% followed by 30% sucrose/PBS solution overnight at 4 °C. Brains were embedded in an OCT cryomount (Histolab Products AB), frozen on dry ice, and sectioned at 20 µm using a cryostat (1850UV, Leica Biosystems). From each brain, coronal sections were obtained (bregma AP +1.42 to −0.46; Franklin and Paxinos 2008) and divided into 10 series (kept at −20 °C). One series per mouse was used in each experiment, resulting in the analysis of brain sections throughout the striatum with a 200-µm sampling interval.

Immunohistochemistry

Sections were washed in PBS and incubated in a blocking solution (10% normal goat serum, 2.5% BSA, 0.5 M NaCl, and 0.3% Tween 20 in PBS) for 1 h at room temperature. They were then incubated in primary antibodies in dilution buffer (2.5% BSA, 0.5 M NaCl, and 0.3% Tween 20 in PBS) overnight at 4 °C, washed in PBS 4 times for 10 min each and 1 h of secondary antibody incubation at room temperature, followed by 4 washes in PBS for 5 min each. Nuclear counterstaining was performed with 100 ng/mL of 4,6-diamidino-2-phenylindole (DAPI) solution in water for 10 min. Primary antibodies were used at the following concentrations: chicken anti-green fluorescent protein (1 : 2000, Abcam), mouse anti-PV (1 : 1000; Sigma-Aldrich), rat anti-SST (1 : 500; Millipore Bioscience Research Reagents), rabbit anti-neuropeptide Y (1 : 2000; Diasorin), rabbit anti-CR (1 : 1000; Swant), mouse anti-reelin (1 : 500; MBL), rat anti-chicken ovalbumin upstream promoter-transcription factor-interacting protein 2 (Ctip2; 1 : 500, Abcam), sheep anti-nNOS (1:10 000; Herbison et al. 1996), rabbit anti-TH (1 : 1000, Pel-Freez), and rabbit anti-vasoactive intestinal polypeptide (1 : 500, Incstar). Secondary antibodies conjugated with Cy3 and Cy5 (1 : 200; Jackson ImmunoResearch) or Alexa Fluor dyes 488, 594, and 647 (1 : 1000; Invitrogen) were used to visualize the signals. TSA Plus Cyanine 3/Fluorescein System (PerkinElmer) was used to amplify the signal with the nNOS antibody according to the manufacturer's instructions. In each slice, 2 square confocal images (with 10 µm optical sections, ×10 magnification, zoom 0.6 one in each hemisphere) of the dorsolateral striatum containing typically 40–100 EGFP^{+} cells were taken using a Zeiss LSM 700 microscope. Only cells with clearly distinguishable nuclei were counted.

Double In Situ Hybridization

In situ hybridization with a digoxigenin full-length cDNA probe of Gad67 was performed as previously described (Lee et al. 2010). The digoxigenin probe was detected using the TSA Plus Cy3 system (PerkinElmer, USA) with an anti-DIG-HRP antibody, followed by immunohistochemistry against EGFP in 5HT3a[EGFP] mice (see immunohistochemistry). Images were obtained as described above by confocal microscopy.

6-Hydroxydopamine Lesion

5HT3a[EGFP] mice received a unilateral injection of 6-hydroxydopamine (6-OHDA, Sigma-Aldrich) in the substantia nigra pars compacta (SNc). Mice were anesthetized in an induction chamber under 1.5–2% isoflurane using O_2 as carrier gas. Following shaving and cleaning of the surgical area, the animal was placed in a stereotaxic frame (Kopf Instruments) and anesthesia was maintained under 1.5–2% isoflurane in O_2. "Bregma" was exposed via incision of the skin, and a small burr hole was created using a dental drill to which the lesion cannula was lowered to reach the SNc using these stereotaxic coordinates: AP −3.0, mediolateral −1.2, and dorsoventral −4.5 mm. The nose bar was set at 0.0 mm. 6-OHDA was administered at a concentration of 3 µg/µL dissolved in 0.9% sterile saline with 0.2 mg/mL of ascorbic acid, injecting 1 µL/mouse at a rate of 0.3 µL/min with a 30-gauge steel cannula connected via polyethylene tubing to a 10-µL Hamilton syringe mounted on a micro-drive pump.

Electrophysiological Recordings

Whole-cell patch-clamp electrophysiological recordings were obtained from EGFP-expressing cells in acute brain slices prepared from P16 to P34 animals. Animals were anesthetized deeply with isoflurane, decapitated, and the brain was quickly removed and transferred to ice-cold artificial cerebrospinal fluid (aCSF) of the following composition (in mM): 125 NaCl, 2.5 KCl, 25 NaHCO$_3$, 1.25 NaH$_2$PO$_4$, 1 MgCl$_2$, 2 CaCl$_2$, and 20 glucose. The brain was then fixed to a stage and 250–300 µm slices were cut on a vibratome (VT1200 S, Leica). Slices were then individually transferred into an incubation chamber containing oxygenated aCSF at room temperature for a minimum period of 1 h before recordings. Alternatively, the slices were incubated at 35 °C for 30–60 min and then transferred to room temperature (22–25 °C). During recording, slices were continually perfused with oxygenated aCSF of the same composition and kept at room temperature or 34 ± 0.5 °C. Patch electrodes were made from borosilicate glass (resistance 5–10 MΩ; Hilgenberg, GmbH) and filled with a solution containing (in mM): 128 K-gluconate, 4 NaCl, 0.3 Mg-GTP, 5 Na-ATP, 10 HEPES, 1 glucose, and 5 mg/mL of biocytin (Sigma) or 105 K-gluconate, 30 KCl, 10 Na-Phosphocreatine, 10 HEPES, 4 Mg-ATP, 0.3 Na-GTP, and 5 mg/mL of biocytin (Sigma). All recordings were performed in current-clamp mode, using EPC10 (HEKA) or Multiclamp 700B (Molecular Devices) amplifiers, and analyzed off-line in Clampfit v.10.2 and IGOR Pro (Wavemetrics). Perforated patch-clamp recordings were obtained using pipettes containing (in mM): 140 K-methylsulfate, 10 HEPES, 0.2 EGTA, 7.5 NaCl, 2 Mg-ATP, and 0.2 Na-GTP. Gramicidin-D was added from a stock solution of 0.5 mg/mL in DMSO to achieve a final concentration of 0.5–1 µg/mL in the pipette solution. At the end of these experiments, the membrane was ruptured to fill the recorded cell with biocytin.

For pharmacological stimulation, 100 µM nicotine ditartrate (Tocris Bioscience) was applied directly onto the soma of the recorded cell by puffing (30 ms, using a Picospritzer-III device; Parker Hannifin) through a second patch pipette located 10–30 µm away from the soma. Extracellular solution contained the glutamatergic α-Amino-3-hydroxy-5-methyl-4-isoxazolepropionic acid/kainate and *N*-methyl-D-aspartate (NMDA) receptor antagonists (6-cyano-7-nitroquinoxaline-2,3-dione and (2*R*)-amino-5-phosphonovaleric acid; (2*R*)-amino-5-phosphono-pentanoate; Sigma-Aldrich) and a GABA-A antagonist (gabazine;

Sigma) was also applied to ensure that responses to nicotine were direct and not mediated by polysynaptic transmission. All blockers were used at a final concentration of 10 μM. Following recordings, slices were fixated in 4% paraformaldehyde and then cryoprotected in a 30% sucrose solution in PBS, frozen, and resectioned to 50 μm thickness with a sledge microtome. The sections were rinsed in PBS and incubated in Alexa 594-conjugated streptavidin (1 : 200 in PBS with 0.1% Triton X-100) for at least 2 h. The sections were then rinsed 5 times in PBS (at least 15 min per rinse), mounted on slides using the Fluoromount-G medium (Southern Biotech), and coverslipped. Labeled cells were subsequently imaged by confocal or two-photon microscopy.

Measurement of Intrinsic Properties

Depolarizing and hyperpolarizing current steps were used to extract the following electrical properties of recorded neurons: The resting membrane potential (RMP) was measured momentarily after membrane rupture; input resistance (R_{in}) was obtained by the steady-state voltage response to a hyperpolarizing current step injection; membrane time constant (τ_m) was extracted by performing an exponential fit to the decay phase of a voltage response to a negative current step; H-current-mediated sag was measured as the voltage difference between the peak hyperpolarization and the steady-state response to a long (1 s) current step. The AP threshold was obtained from the first AP discharge during a ramp current injection (from 0 pA to ~2 times threshold current, over 3 s). The additional following parameters were measured from the same protocol: AP amplitude; AP width at half amplitude; and after-hyperpolarization (AHP) latency (the time from spike threshold to lowest point of the AHP).

Statistical Analyses of Intrinsic Properties

All data were analyzed for statistical significance using the SPSS (v.17) software package (IBM, Chicago, IL, USA). We utilized informal cut-offs to categorize the population heterogeneity and conducted several rounds of supervised clustering based on key measures of intrinsic properties to classify cells into subgroups with similar physiological profiles. Principle component analysis with varimax rotation was used to extract groups of measurements based on their linear correlation, and stepwise regression analysis was used to determine which components predicted subgroup classification. All data were then analyzed for between-group statistical significance using multivariate analysis of variance (ANOVA) to examine overall differences between the groups. Post hoc independent-sample t-tests with Bonferroni's correction for multiple comparisons were then conducted to examine differences between individual subgroups.

Results

5HT3a[EGFP] Labels a Large Striatal GABAergic Population That Does Not Include MSNs

Using a transgenic mouse line that expresses EGFP under the 5HT3a promoter, we observed labeled cells throughout the striatum (Fig. 1A). All EGFP^{+} cells were GABAergic (100%, $n = 4$ animals, >100 cells per animal), as shown by in situ hybridization for Gad1 combined with immunohistochemistry against EGFP (Fig. 1B). While $6.84 \pm 1.58\%$ ($n = 7$ animals) of EGFP^{+} cells were labeled by the MSN marker Ctip2 (Arlotta et al. 2008), double immunofluorescence revealed no overlap with DARPP-32, another MSN marker, in EGFP-expressing cells (Fig. 1B,C). Furthermore, the EGFP/Ctip2 double-positive neurons never exhibited spiny dendrites (Supplementary Fig. 1), arguing that Ctip2 is not specific to MSNs ($n = 15$ cells). Moreover, we have never observed spiny dendrites on Ctip2-negative EGFP^{+} cells, we could not detect EGFP[+] axons in the globus pallidus, nor did we observe retrogradely labeled EGFP^{+} cells after injection of fluorescently labeled beads into the substantia nigra ($n = 3$, data not shown) further indicating that all EGFP+ cells are indeed interneurons.

To assess the proportional contribution of the 5HT3a[EGFP] population, we counted EGFP-expressing cells in the dorsolateral striatum as compared to the number of MSNs (Ctip2^{+}/EGFP[−]) in the same area. The percentage of 5HT3a[EGFP] cells was $3.74 \pm 0.64\%$ ($n = 7$ animals) relative to the MSN population.

Quantitative Assessment of Molecular Marker Expression in the Striatal GABAergic Interneuron Population

With the aim of creating a comprehensive map of the novel, as well as known interneuron populations in the dorsolateral striatum, we used double and triple labeling against known
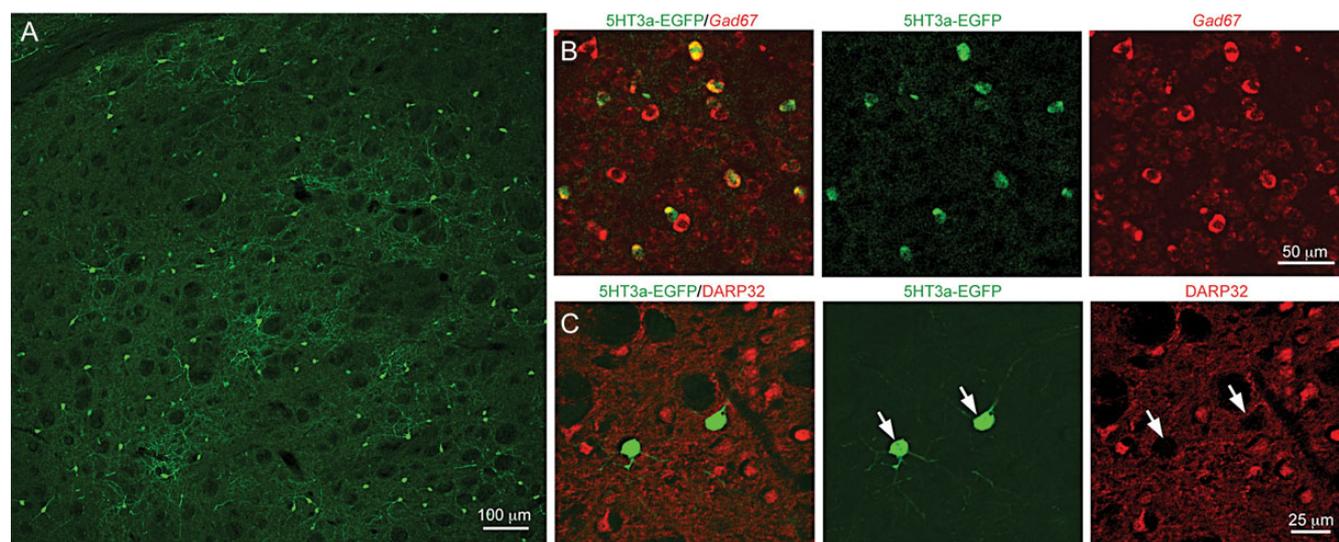

Figure 1. 5HT3a[EGFP] mouse labels a population of striatal GABAergic interneurons. (A) Immunofluorescence for EGFP shows the dorsolateral striatal 5HT3a[EGFP]-expressing population. (B) Double immunohistochemistry for EGFP and in situ hybridization for Gad67, respectively. Note that all 5HT3a[EGFP] cells are also Gad67 positive. (C) Double immunohistochemical staining for medium-sized spiny neuron (MSN) marker DARPP32 and EGFP show that cells labeled in the 5HT3a[EGFP] mouse are not MSN cells.

Table 1
Overlap and relative contribution of molecular markers for striatal gINs

Marker	Proportion of total gIN population (%)	% of 5HT3a^{EGFP} population-expressing marker	% of marker population-expressing EGFP
PV	13.68	19.8 ± 0.3	46.98 ± 0.24
nNOS	16.93	0	0
SST	15.23	0.11 ± 0.11	0.38 ± 0.38
NPY	16.27	1.67 ± 0.48	4.63 ± 1.11
TH	2.58	2.48 ± 0.51	26.45 ± 1.02
CR	2.06	1.51 ± 0.27	24.64 ± 1.22
5HT3a^{EGFP}	33.24	—	100

striatal gIN markers and quantified the overlap with 5HT3a^{EGFP} cells. Because we had already quantified the proportion of EGFP$^+$ cells relative to MSNs, we counted PV-, TH-, CR-, SST-, nNOS- and NPY-positive cells relative to EGFP$^+$ cells to determine the proportional contribution of each population (summarized in Table 1). We saw very little overlap with the markers SST, nNOS, NPY, and CR (Fig. 2*B–E*, for single-fluorescent channels see Supplementary Fig. 2). However, $19.78 \pm 0.26\%$ of the EGFP$^+$ population expressed PV ($n = 3$ animals; Fig. 2*A*). In order to refine our molecular interneuron map, we also studied the relative contribution of and overlap between the SST, NPY, and nNOS populations (Fig. 2*B,F*). Another previously described population of gINs expresses TH but at levels too low to be detected by immunohistochemistry. These neurons are, however, detectable in the TH^{EGFP} mouse or by reducing the surrounding levels of TH in striatum via a 6-OHDA lesion in the SNc (Jollivet et al. 2004; Darmopil et al. 2008; Ibanez-Sandoval et al. 2010). In order to elucidate if the EGFP$^+$ population in this study overlaps with the TH population, we performed unilateral 6-OHDA lesions in the SNc of 5HT3a^{EGFP} mice. One week after injection, we quantified our lesions by immunohistochemistry for TH in the striatum and SNc (Supplementary Fig. 3) and performed double immunohistochemistry against TH and EGFP in the striatum. The number of EGFP-positive cells per field of view did not differ between lesioned and non-lesioned hemispheres (68.60 ± 0.99 vs. 68.20 ± 1.18, $n = 5$ animals, $P = 0.96$), but the number of detectable TH-immunoreactive cells increased significantly on the lesioned side (9.44 ± 0.47 vs. 2.80 ± 0.48, $n = 5$, $P = 0.004$, two-tailed Student's t-test). A small fraction of EGFP-positive cells in the dopamine-depleted striatum were also TH-immunoreactive ($2.48 \pm 0.51\%$; Fig. 2*E*). We did not quantify the mutual overlap between TH, CR, and PV with any other marker than EGFP, since these markers have been shown to be non-overlapping (Ibanez-Sandoval et al. 2010; Tepper et al. 2010). We used this molecular characterization of striatal interneuron populations to create a diagram in which the proportion of cells expressing each marker and overlap between markers are represented as area (Fig. 2*F*).

In order to reconcile the previously described morphological data with our molecular map, and to determine how large the gIN populations were, we also calculated the relative combined contribution of all populations identified by interneuron markers when compared with the numbers of MSNs (Ctip2$^+$/EGFP$^-$ cells). We found that the cumulative total of all stained gIN populations equates to 4.46% of all neurons in the dorsolateral striatum. Given that cholinergic neurons (0.4–1.5%) were excluded from this analysis, this result is in close range to the 5% of interneurons in the striatum as identified by nuclear morphology (Graveland and DiFiglia 1985).

5HT3a^{EGFP} Cells Have Heterogeneous Electrophysiological Properties

In order to address the diversity in the population labeled in the 5HT3a^{EGFP} mouse, we obtained current-clamp recordings of intrinsic properties of 129 EGFP$^+$ neurons. Whole-cell or perforated patch (to reveal spontaneous activity) recordings showed that the EGFP$^+$ population was highly heterogeneous both with regard to intrinsic firing properties and morphology. Quantification of intrinsic properties is summarized in Table 2. Based on the properties of recorded neurons (see Materials and Methods and further description below), we defined 3 subtypes in this population, which we named 5HT3a^{EGFP} Types I–III. Three different intracellular solutions were used in these experiments, but there was no significant effect on intrinsic properties within subtypes and the results were therefore pooled. While Type I and Type II 5HT3a^{EGFP} interneurons were largely homogeneous and reminiscent of previously described cell types, Type III demonstrated substantial variability. None of the recorded EGFP$^+$ neurons had firing properties resembling MSNs or cholinergic interneurons. Representative examples of the intrinsic properties of each subtype are shown in Figure 3*A*$^{1–3}$.

We further analyzed the intrinsic membrane properties of recorded EGFP$^+$ cells for between-subtype differences. Overall, multivariate ANOVA demonstrated main effects of subtype on AHP amplitude ($F_{2,55} = 16.53$, $P < 0.001$) and latency ($F_{2,55} = 4.64$, $P = 0.02$), RMP (V_{rest}; $F_{2,55} = 9.09$, $P < 0.001$), I_H (sag; $F_{2,55} = 11.03$, $P < 0.001$), membrane time constant (tau; $F_{2,55} = 12.75$, $P < 0.001$), rebound depolarization ($F_{2,55} = 8.40$, $P < 0.001$), and input resistance (IR: $F_{2,55} = 10.50$, $P < 0.001$). To dissect differences between the 3 subtypes, one-way ANOVA with Bonferroni's correction for multiple comparisons was performed for each parameter. All but 3 comparisons were significantly different between groups; AP threshold was similar in all 3 groups, AHP latency was the same for Type II and Type III cells, and the AP amplitude of Type I and Type III cells were not statistically different. The results of post hoc statistical analyses are described in Supplementary Table 1.

Type I cells (32%, $n = 41$ cells) exhibited properties typical of FS interneurons, including short AP half-width, low input resistance, deep AHP, a high maximum firing rate, and non-accommodating, often stuttering, firing (Fig. 3*A*^{1}). These cells were indistinguishable from FS cells labeled in the Lhx6^{EGFP} mouse line (Cobos et al. 2006), and a pair of 5HT3a^{EGFP+} FS cells was electrically coupled during dual recordings, suggesting that these are indeed typical PV-expressing FS cells (Koos and Tepper 1999; Gittis et al. 2010; Supplementary Fig. 4). Type II cells (16%; $n = 20$ cells) exhibited delayed firing at and above threshold with a ramp leading up to the first AP. They also had slightly larger AP half-widths with a slower, more rounded AHP and an accommodating firing pattern (Fig. 3*A*^{2}). Type II cells exhibited significantly longer AHP latencies compared with Type I cells (Fig. 3*B*^{5}), and the firing pattern was reminiscent of both striatal NPY-expressing NGF cells (Ibanez-Sandoval et al. 2011; English et al. 2012) and cortical 5HT3a-expressing late-spiking LS1 cells, which also have NGF-like morphologies (Lee et al. 2010). Type III cells were the most frequently observed subgroup of 5HT3a^{EGFP} cells, constituting 53% of the total striatal EGFP$^+$ population ($n = 68/129$ cells). The Type III subgroup was a diverse non-FS/non-NGF population with some LTS-like properties (Fig. 3*A*^{3}).
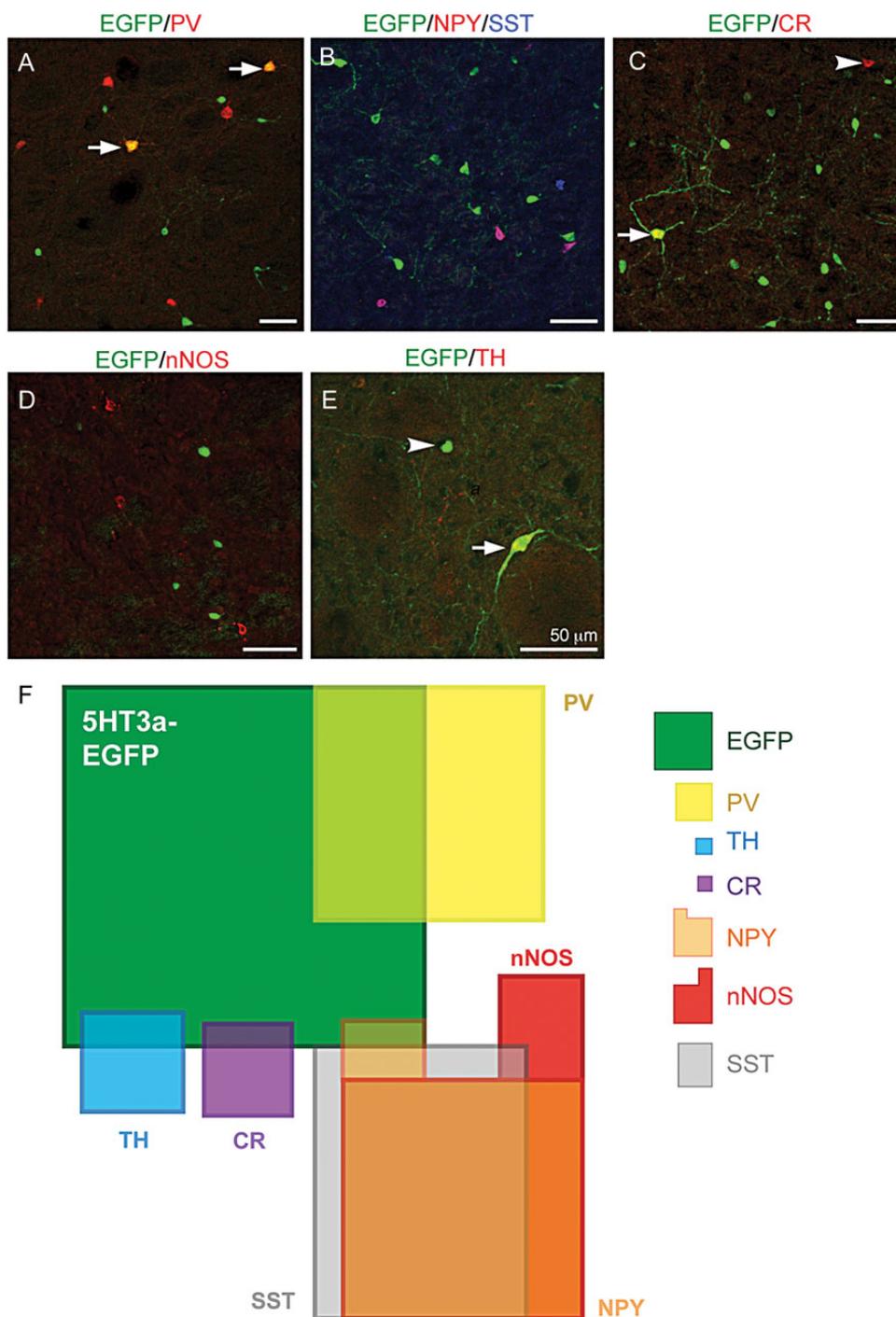
Figure 2. A majority of striatal 5HT3a[EGFP] cells do not overlap with known interneuron markers. (*A–E*) Double and triple immunohistochemical staining of the dorsolateral striatal 5HT3a[EGFP] population for EGFP and (*A*) PV, (*B*) NPY and SST (NPY/SST), (*C*) CR, (*D*) nNOS, and (*E*) TH (in a 6-OHDA-lesioned striatum). Arrows and arrowheads mark double-positive neurons and single-positive neurons, respectively. (*F*) A schematic of the populations expressing known striatal interneuron markers including those labeled in the 5HT3a[EGFP] mouse. The area of each box, including all overlaps, is proportional to the relative contributions found in our study (see Table 1 for detailed description). On the right side is the legend showing the relative size, color and shape of the described cell populations in the map.

For example, a proportion of Type III cells exhibited an initial burst of AP at threshold (21%) as often seen in the typical SST/NPY pLTS cells, while some Type III cells exhibited an LTS AHP (24%), and 32% of Type III cells (*n* = 6/19 cells) demonstrated spontaneous activity during perforated patch, with a frequency of 11.2 ± 1.2 Hz. The RMP, input resistance, and membrane time constant were all significantly higher in Type III cells compared with the other 2 subgroups (Fig. 3B[1,3,4]).

Heterogeneity of 5HT3a[EGFP] Cells Is Reflected in Cell Morphologies

During some of the electrophysiological recordings, we included biocytin or neurobiotin in the gramicidin-containing intracellular solution to recover examples of cell morphologies from each of the 3 subtypes (Fig. 4). None of the EGFP^{+} cells examined demonstrated spiny dendrites, characteristic of MSN cells (Supplementary Fig. 1). Although small sample sizes

Table 2
Intrinsic properties for interneurons labeled by 5HT3a[EGFP]

Parameters measured	Type I (n = 41)	Type II (n = 20)	Type III (n = 68)
AP threshold (mV)	−40.23 ± 1.04	−38.29 ± 1.29	−39.34 ± 0.81
AP half-width (ms)	0.60 ± 0.1	0.97 ± 0.09	0.89 ± 0.08
AP amplitude (mV)	53.59 ± 2.96	58.22 ± 3.45	62.77 ± 1.69
AHP amplitude (mV)	20.47 ± 1.96	16.26 ± 1.37	11.57 ± 0.68
AHP latency (ms)	1.51 ± 0.20	9.37 ± 1.65	4.82 ± 0.93
V_{rest} (mV)	−73.64 ± 1.85	−71.76 ± 1.80	−64.84 ± 1.21
Sag (mV)	0.92 ± 0.33	0.53 ± 0.09	2.97 ± 0.39
Rebound depolarization (mV)	−0.47 ± 0.22	−0.34 ± 0.19	−1.89 ± 0.32
Input resistance (MΩ)	123.86 ± 12.87	215.95 ± 29.29	386.51 ± 38.01
Membrane time constant (τ)	6.57 ± 1.33	12.69 ± 2.05	23.19 ± 1.96
Spontaneous activity (%)	0	25.0	31.6
Low-threshold spike (%)	0	0	23.5
Subthreshold oscillations (%)	31.6	72.0	13.0

Mean ± SEM for Type I, II, and III cells.

precluded statistical analysis, the subtypes showed clear differences in morphology. The EGFP[+] Type I cells (n = 6) had medium-sized somas and compact dendritic and axonal branching (Fig. 4A_1), much like typical PV–FS basket cells. Likewise, the EGFP[+] Type II cells (n = 2) showed the dense and extensive dendritic branching close to the soma (Fig. 4B_1), similar to the previously described NPY–NGF cells (Ibanez-Sandoval et al. 2011). A wide-stretched dendritic tree characterized EGFP[+] Type III morphologies (n = 5), with 2–3 primary dendrites arranged in a longitudinal manner (Fig. 4C_1). To determine soma size in these cells, we measured the vertical axis of cells with a clear nucleus on confocal images of 5HT3a[EGFP] sections immunostained for EGFP with DAPI as a nuclear counterstain (230 neurons from 3 animals; Fig. 4D). This analysis revealed that a majority of cells are indeed medium sized (8–13 μm), but that there is considerable diversity. This diversity probably reflects the heterogeneity of cell types, but may also stem from randomly oriented elongated Type III cells.

5HT3a Cells Are Molecularly and Pharmacologically Distinct

We probed the pharmacological response of the 3 different 5HT3a[EGFP] subtypes to the cholinergic agonist nicotine. None of the Type I cells (0/13) and only 25% (2/8) Type II cells responded with a depolarization when puffed with 100 μM nicotine. Conversely, a majority of the Type III cells (86%, n = 18/21) responded with a robust depolarization often causing firing of multiple APs, following a brief (30 ms) pulse of nicotine. To compare these findings with known subtypes, we also applied nicotine to PV-expressing FS cells and NPY/SST-expressing LTS cells in slices from Lhx6[EGFP] mice (Gittis et al. 2010). We observed one very small response in an FS cell and only 27% (4/15) in the LTS-like cells (Fig. 5). The magnitude of responses in Lhx6[EGFP] LTS cells was significantly lower with no cell reaching discharge threshold, while 14/18 5HT3a[EGFP] Type III cells responded with AP discharge (Fig. 5B).

Discussion

The 5HT3a[EGFP] Population Reconciles Disparate Estimates of Interneuron Numbers in the Striatum

Here we present evidence for 2 novel populations of gINs in the dorsolateral striatum. The relative contribution of gINs

labeled in the 5HT3a[EGFP] mouse is almost as large as the cumulative sum of all previously described populations and brings the total percentage of molecularly defined gINs up to that originally proposed by morphological studies (Graveland and Di-Figlia 1985). In addition to the 3 larger classical molecular subtype divisions in the striatum (NPY/SST/nNOS, PV, and ChAT), and the more recently discovered TH (Tepper et al. 2010) and NPY–NGF populations, the present study proposes at least 2 novel distinct striatal subtypes, namely the NPY-negative LS-NGF cell type (Type II) and the SST/NPY/nNOS-negative LTS-like cell type (Type III). The relative contribution of the PV-, CR- and TH-negative 5HT3a[EGFP] cell population maps precisely onto the missing proportion of interneurons that were described by the assessment of nuclear morphology, but remained unaccounted for by known markers (Luk and Sadikot 2001; Rymar et al. 2004; Tepper et al. 2010). Therefore, it appears likely that the field is now close to identifying the full spectrum of striatal interneuron subtypes.

Striatal gINs Exhibit Substantial Molecular and Electrophysiological Heterogeneity

We demonstrate that an unexpectedly large variety of interneuron subtypes exists in the striatum. The striatal interneurons labeled by 5HT3a[EGFP] were heterogeneous and exhibited 3 distinct electrophysiological and morphological profiles that were similar to previously reported populations. However, their molecular and pharmacological profiles showed that groups II and III were distinct from previously known populations. The PV-expressing EGFP^{+} cells appeared in all respects to be classical FS cells and did not differ significantly in electrophysiological and/or molecular parameters from previously described FS interneurons (Koos and Tepper 1999; Gittis et al. 2010). We also describe a novel LS-NGF cell type that did not express the classical marker NPY and did not respond reliably to the application of nicotine. This is in stark contrast to the previously described NPY–NGF cell that inhibits MSN cells upon cholinergic activation of nAChRs (Ibanez-Sandoval et al. 2011; English et al. 2012). Likewise, while the Type III cells described in this study were electrophysiologically and morphologically similar to the classical NPY/SST/nNOS LTS cells, they differ in the expression of all 3 markers as well as demonstrating strikingly more pronounced responses to activation of nAChRs. It is worth noting here that overlap with NPY expression may vary over time given that NPY expression is activity-dependent in cortical interneurons (Baraban et al. 1997; Wirth et al. 1998) and is induced in striatal neurons not normally expressing NPY upon injections of methamphetamine (Horner et al. 2006). The differences in response to activation of nAChRs, however, would suggest that these 2 populations of NGF cells partake in distinct striatal sub-circuits. A similar functional dichotomy exists between 5HT3a-positive and -negative oriens lacunosum-moleculare cells in the hippocampus (Chittajallu et al. 2013). In the rat, FS cells have been shown to be activated by puffing with nAChR agonists including 250 μM nicotine (Koos and Tepper 2002). In contrast to this, we rarely observed any nicotine-induced responses in EGFP^{+} FS cells (Type I) or in FS cells labeled in the Lhx6[EGFP] mouse. This discrepancy could be due to species differences or to experimental differences, such as the concentration of agonists. We did see a modest overlap between EGFP and the markers TH, CR, and NPY (in total 5.66% of EGFP^{+} cells), and it is likely that these cells were
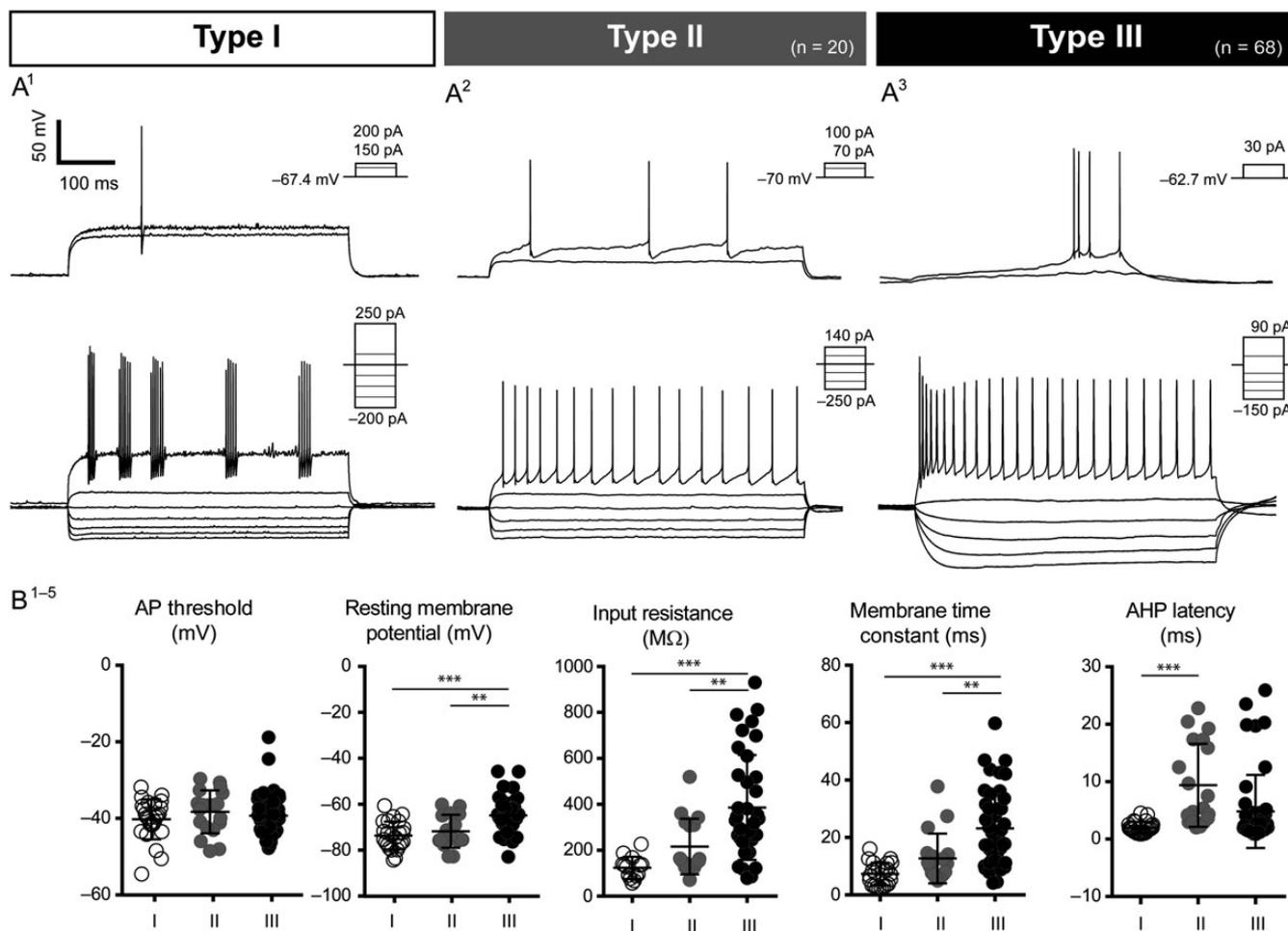
Figure 3. Electrophysiological profiles of 5HT3a^{EGFP} cells. Three distinct subtypes were discovered within the 5HT3a^{EGFP} population. Type 1 cells exhibited properties typical of FS cells, with short AP half-widths and fast and deep AHPs (A^1). Type II cells were very similar to the previously described NGF cells, both in terms of physiology and morphology (A^2). Type III cells (A^3) formed the largest subgroup and was also the most heterogeneous, exhibiting a range of specific features not seen in the other 2 groups. Multivariate ANOVAs and post hoc multiple comparisons demonstrated that a number of measured parameters were able to differentiate the 3 subgroups successfully. While the threshold for AP activation did not differ between groups (B^1), Type III cells had significantly different RMP s, membrane time constants, and input resistances, compared with both Type I and II cells (B^{2-4}). The features that best distinguished Type I and Type II cells were related to temporal properties of AP discharge, for example, Type II cells exhibited longer AHP latencies than did Type I cells (B^5).

electrophysiologically classified within the Type II and III groups. This small overlap may explain the infrequent response to nicotine observed in Type II EGFP cells and the proportion of Type III cells that failed to respond to nicotine.

While the sheer number of non-MSN cells labeled in the 5HT3a^{EGFP} mouse raises the question of how these cells have escaped detection, it is clear upon examining recordings that, at first pass, most of the novel cells in groups II and III could be classified as typical LTS or NGF cells. It was only by combining marker expression with pharmacological characterization that we were able to detect the difference.

Developmental Origin of Striatal 5HT3a^{EGFP} Neurons

Inhibitory telencephalic structures such as the striatum and the central nucleus of the amygdala have been assumed to be populated by gINs derived solely from the MGE or the POA (Fishell and Rudy 2011). Striatal projection neurons are derived from the LGE (Deacon et al. 1994). Transplantation studies have suggested that the CGE also contributes to the striatum in the form of MSNs (Nery et al. 2002), though contributions from LGE cells

migrating through the CGE at the time of transplantation could not be ruled out. Since all 5HT3a-expressing gINs in the cortex and the hippocampus are CGE-derived, the findings of this study challenge the hypothesis that the CGE exclusively contributes gINs to excitatory telencephalic structures (Lee et al. 2010; Tricoire et al. 2011). Whether striatal 5HT3a^{EGFP} cells originate from the CGE remains to be shown directly. Since no genetic fate mapping strategy exists to exclusively label striatal CGE-derived cells, a deductive fate mapping strategy could be employed using Lhx6^{cre} or Nkx2-1^{cre} to label MGE-derived cells and assess the overlap with 5HT3a^{EGFP}.

Putative Function of 5HT3a^{EGFP} Interneurons in Striatal Cholinergic Tone

It has been shown that all cortical interneurons labeled in the 5HT3a^{EGFP} mouse express functional 5-HT$_3$ receptors (Lee et al. 2010), and that at least a majority of labeled cells in the hippocampus have the *htr3a* mRNA as shown by single-cell reverse transcription PCR (Tricoire et al. 2011). However, since the 5HT3a^{EGFP} line is a BAC-transgenic mouse, the faithful
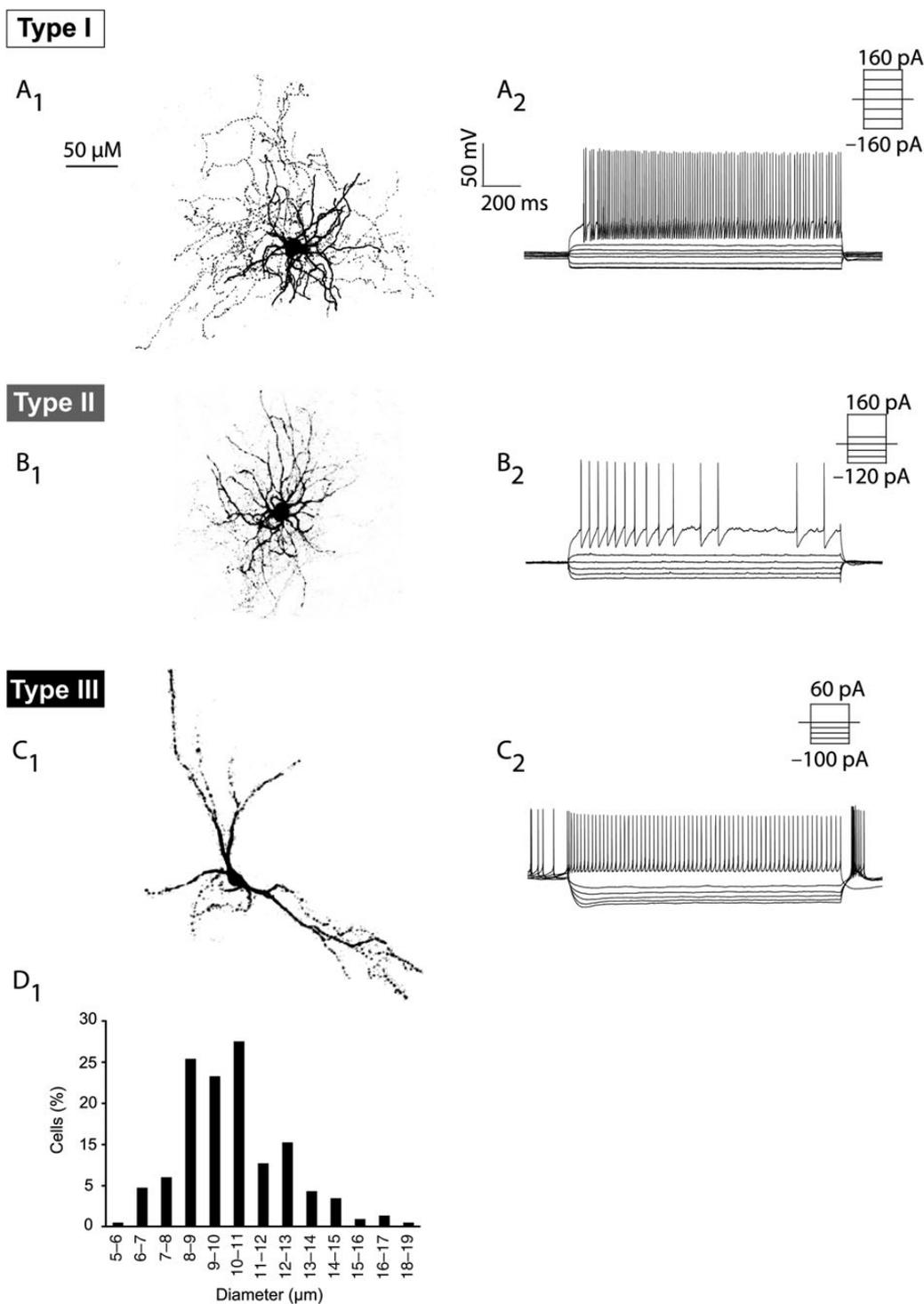
Figure 4. Morphology of the 5HT3a^{EGFP} interneuron subtypes. Examples of different morphologies of 5HT3a^{EGFP} gINs (A_1–C_1) and their corresponding electrophysiological recordings (A_2–C_2). (A) Type I interneurons had medium-sized somas and compact dendritic and axonal branching (A_1) and exhibited typical FS properties (A_2). (B) A LS-NGF cell (Type II) exhibiting a typical NGF morphology with dense and extensive dendritic branching close to the soma (B_1). These cells exhibited some characteristics similar to FS cells, but had a larger input resistance and pronounced intraspike interval adaptation (B_2). (C) An example of a Type III cell with spontaneous activity and a pronounced sag, which exhibited morphology with 2–3 main dendrites and a longitudinally stretched out dendritic tree. (D) The soma size of EGFP$^+$ cells was quantified to demonstrate their medium-size and diversity.

expression of the reporter might not hold true in all parts of the brain including the striatum. This warrants caution in the interpretation of the results of this study beyond using EGFP as a marker for the 2 novel populations.

The 5-HT$_3$ receptor belongs to the cation-selective Cys loop receptor family closely related to the nAChRs (Maricq et al. 1991). 5HT3a subunits can form pentameric pseudosymmetric channels with itself (homomeric) or with the 5HT3b subunit
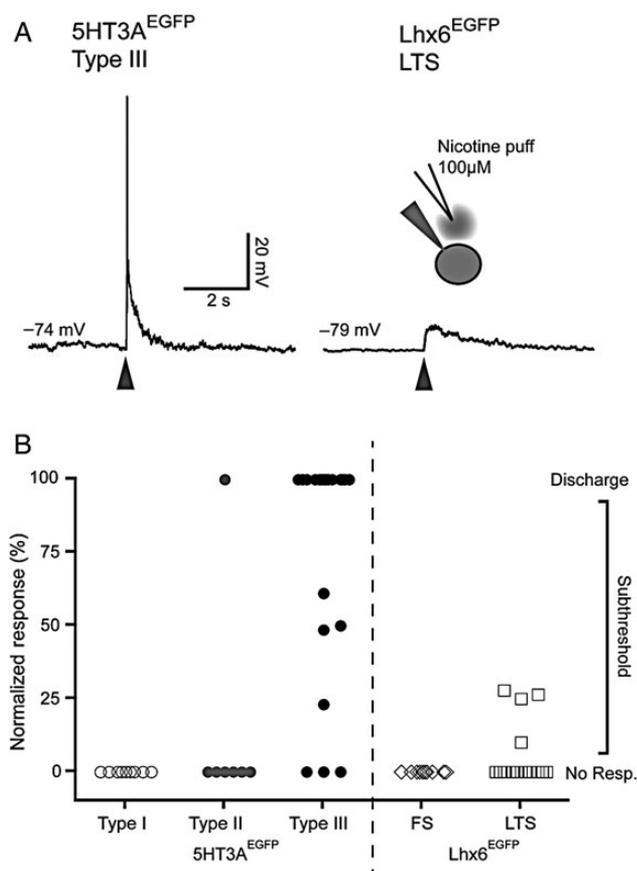
Figure 5. Type III 5HT3a^{EGFP} interneurons are robustly activated by nicotine. (*A*) Representative traces of responses to puffing with 100 μM nicotine ditartate on a Type I 5HT3a^{EGFP} cell (left) and a Lhx6^{EGFP} LTS cell (right). (*B*) Graph representing the normalized response to nicotine puffing in the different cell types labeled in 5HT3a^{EGFP} and Lhx6^{EGFP} mice. Peak of responses were scaled between RMP (0%) and threshold (100%), meaning that any cell that fired in response to puffing was 100%. Note that a majority of 5HT3a^{EGFP} Type III cells responded strongly, while only scattered responses was seen in some other cell types.

5HT3a^{EGFP} population is involved in the synchronization of ChAT cells, and that this phenomenon can be initiated by a fast long-range serotonergic signal.

Understanding the cellular diversity is a prerequisite for understanding the intricate wiring scheme of any brain structure. Until now, cellular diversity within the striatum was thought to be much smaller than in other telencephalic structures, such as the well-studied neocortex and hippocampus. The data presented in this paper demonstrate a large heterogeneity in striatal interneuron types and raise the intriguing possibility that striatal interneuron classes may be more closely homologous to cortical interneuron classes than previously thought. Further investigation along these lines will undoubtedly facilitate our understanding of integration and processing of information of signals in the basal ganglia.

Supplementary Material

Supplementary material can be found at: http://www.cercor.oxford journals.org/.

Funding

Notes

References

Arlotta P, Molyneaux BJ, Jabaudon D, Yoshida Y, Macklis JD. 2008. Ctip2 controls the differentiation of medium spiny neurons and the establishment of the cellular architecture of the striatum. J Neurosci. 28(3):622–632.

Baraban SC, Hollopeter G, Erickson JC, Schwartzkroin PA, Palmiter RD. 1997. Knock-out mice reveal a critical antiepileptic role for neuropeptide Y. J Neurosci. 17(23):8927–8936.

Blandina P, Goldfarb J, Craddock-Royal B, Green JP. 1989. Release of endogenous dopamine by stimulation of 5-hydroxytryptamine3 receptors in rat striatum. J Pharmacol Exp Ther. 251(3):803–809.

Bolam JP, Clarke DJ, Smith AD, Somogyi P. 1983. A type of aspiny neuron in the rat neostriatum accumulates [3H]gamma-aminobutyric acid: combination of Golgi-staining, autoradiography, and electron microscopy. J Comp Neurol. 213(2):121–134.

Chittajallu R, Craig MT, McFarland A, Yuan X, Gerfen S, Tricoire L, Erkkila B, Barron SC, Lopez CM, Liang BJ et al. 2013. Dual origins of functionally distinct O-LM interneurons revealed by differential 5-HT3AR expression. Nat Neurosci. 16(11):1598–1607.

Cobos I, Long JE, Thwin MT, Rubenstein JL. 2006. Cellular patterns of transcription factor expression in developing cortical interneurons. Cereb Cortex. 16 (Suppl 1):i82–i88.

Darmopil S, Muneton-Gomez VC, de Ceballos ML, Bernson M, Moratalla R. 2008. Tyrosine hydroxylase cells appearing in the mouse striatum after dopamine denervation are likely to be projection neurones regulated by L-DOPA. Eur J Neurosci. 27(3):580–592.

(which is not expressed in the murine central nervous system), and is obligatory for 5-HT$_3$ channel formation (Hanna et al. 2000; Morales and Wang 2002). Homomeric 5HT3a 5-HT$_3$ receptors mediate rapidly activating inward currents that desensitize quickly, causing robust depolarization of neurons expressing it upon activation. It is intriguing to think about the functional consequences of the presence of 2 different fast ionotropic receptor types (nAChRs and 5-HT$_3$ receptors) on the described type III interneuron subclass; one activated by local cholinergic input and the other stimulated by long-range serotonergic signaling.

During the last several years, we have seen a drastic increase in our knowledge of intrastriatal connectivity (English et al. 2012; Szydlowski et al. 2013). However, the network basis for many observed phenomena remains unclear, including the burst-pause response and synchronization of cholinergic cells. There is electrophysiological evidence of an unknown GABAergic source providing feedback and lateral inhibition between ChAT cells via activation of nAChRs (Sullivan et al. 2008), and synchronous firing of ChAT cells is sufficient to cause dopamine (DA)-release (Threlfell et al. 2012). Interestingly, pharmacological stimulation of striatal 5-HT$_3$ receptors is enough to cause DA-release in slice experiments (Blandina et al. 1989). It is thus possible that this novel nAChR-expressing

Deacon TW, Pakzaban P, Isacson O. 1994. The lateral ganglionic eminence is the origin of cells committed to striatal phenotypes: neural transplantation and developmental evidence. Brain Res. 668(1–2):211–219.

English DF, Ibanez-Sandoval O, Stark E, Tecuapetla F, Buzsaki G, Deisseroth K, Tepper JM, Koos T. 2012. GABAergic circuits mediate the reinforcement-related signals of striatal cholinergic interneurons. Nat Neurosci. 15(1):123–130.

Fishell G, Rudy B. 2011. Mechanisms of inhibition within the telencephalon: "where the wild things are". Annu Rev Neurosci. 34:535–567.

Fragkouli A, van Wijk NV, Lopes R, Kessaris N, Pachnis V. 2009. LIM homeodomain transcription factor-dependent specification of bipotential MGE progenitors into cholinergic and GABAergic striatal interneurons. Development. 136(22):3841–3851.

Franklin KBJ, Paxinos G. 2008. The mouse brain in stereotaxic coordinates. 3rd ed. Amsterdam: Elsevier.

Gerfen CR, Wilson CJ. 1996. Chapter II: the basal ganglia. In: Swanson LW, Björklund A, Hökfelt T, editors. Handbook of chemical neuroanatomy. Vol. 12: integrated systems of the CNS, part III. Amsterdam: Elsevier. p. 371–468.

Gittis AH, Nelson AB, Thwin MT, Palop JJ, Kreitzer AC. 2010. Distinct roles of GABAergic interneurons in the regulation of striatal output pathways. J Neurosci. 30(6):2223–2234.

Graveland GA, DiFiglia M. 1985. The frequency and distribution of medium-sized neurons with indented nuclei in the primate and rodent neostriatum. Brain Res. 327(1–2):307–311.

Hanna MC, Davies PA, Hales TG, Kirkness EF. 2000. Evidence for expression of heteromeric serotonin 5-HT(3) receptors in rodents. J Neurochem. 75(1):240–247.

Herbison AE, Simonian SX, Norris PJ, Emson PC. 1996. Relationship of neuronal nitric oxide synthase immunoreactivity to GnRH neurons in the ovariectomized and intact female rat. J Neuroendocrinol. 8(1):73–82.

Horner KA, Westwood SC, Hanson GR, Keefe KA. 2006. Multiple high doses of methamphetamine increase the number of preproneuropeptide Y mRNA-expressing neurons in the striatum of rat via a dopamine D1 receptor-dependent mechanism. J Pharmacol Exp Ther. 319(1):414–421.

Ibanez-Sandoval O, Tecuapetla F, Unal B, Shah F, Koos T, Tepper JM. 2010. Electrophysiological and morphological characteristics and synaptic connectivity of tyrosine hydroxylase-expressing neurons in adult mouse striatum. J Neurosci. 30(20):6999–7016.

Ibanez-Sandoval O, Tecuapetla F, Unal B, Shah F, Koos T, Tepper JM. 2011. A novel functionally distinct subtype of striatal neuropeptide Y interneuron. J Neurosci. 31(46):16757–16769.

Iversen LL, Schon FE. 1973. The use of autoradiographic techniques for the identification and mapping of transmitter-specific neurons in the CNS. In: Mandell AJ, editor. New concepts in neurotransmitter regulation. New York: Plenum Press. p. 153–193.

Jollivet C, Montero-Menei CN, Venier-Julienne MC, Sapin A, Benoit JP, Menei P. 2004. Striatal tyrosine hydroxylase immunoreactive neurons are induced by L-dihydroxyphenylalanine and nerve growth factor treatment in 6-hydroxydopamine lesioned rats. Neurosci Lett. 362(2):79–82.

Kawaguchi Y, Wilson CJ, Augood SJ, Emson PC. 1995. Striatal interneurones: chemical, physiological and morphological characterization. Trends Neurosci. 18(12):527–535.

Kita H. 1993. GABAergic circuits of the striatum. Prog Brain Res. 99:51–72.

Kita H, Kitai ST. 1988. Glutamate decarboxylase immunoreactive neurons in rat neostriatum: their morphological types and populations. Brain Res. 447(2):346–352.

Koos T, Tepper JM. 1999. Inhibitory control of neostriatal projection neurons by GABAergic interneurons. Nat Neurosci. 2(5):467–472.

Koos T, Tepper JM. 2002. Dual cholinergic control of fast-spiking interneurons in the neostriatum. J Neurosci. 22(2):529–535.

Lee S, Hjerling-Leffler J, Zagha E, Fishell G, Rudy B. 2010. The largest group of superficial neocortical GABAergic interneurons expresses ionotropic serotonin receptors. J Neurosci. 30(50):16796–16808.

Lindefors N, Brene S, Herrera-Marschitz M, Persson H. 1989. Region specific regulation of glutamic acid decarboxylase mRNA expression by dopamine neurons in rat brain. Exp Brain Res. 77(3):611–620.

Luk KC, Sadikot AF. 2001. GABA promotes survival but not proliferation of parvalbumin-immunoreactive interneurons in rodent neostriatum: an in vivo study with stereology. Neuroscience. 104(1):93–103.

Maricq AV, Peterson AS, Brake AJ, Myers RM, Julius D. 1991. Primary structure and functional expression of the 5HT3 receptor, a serotonin-gated ion channel. Science. 254(5030):432–437.

Morales M, Wang SD. 2002. Differential composition of 5-hydroxytryptamine3 receptors synthesized in the rat CNS and peripheral nervous system. J Neurosci. 22(15):6732–6741.

Nery S, Fishell G, Corbin JG. 2002. The caudal ganglionic eminence is a source of distinct cortical and subcortical cell populations. Nat Neurosci. 5(12):1279–1287.

Oorschot DE. 2013. The percentage of interneurons in the dorsal striatum of the rat, cat, monkey and human: a critique of the evidence. Basal Ganglia. 3(1):19–24.

Phelps PE, Houser CR, Vaughn JE. 1985. Immunocytochemical localization of choline acetyltransferase within the rat neostriatum: a correlated light and electron microscopic study of cholinergic neurons and synapses. J Comp Neurol. 238(3):286–307.

Rubin AN, Alfonsi F, Humphreys MP, Choi CK, Rocha SF, Kessaris N. 2010. The germinal zones of the basal ganglia but not the septum generate GABAergic interneurons for the cortex. J Neurosci. 30(36):12050–12062.

Rudy B, Fishell G, Lee S, Hjerling-Leffler J. 2011. Three groups of interneurons account for nearly 100% of neocortical GABAergic neurons. Dev Neurobiol. 71(1):45–61.

Rymar VV, Sasseville R, Luk KC, Sadikot AF. 2004. Neurogenesis and stereological morphometry of calretinin-immunoreactive GABAergic interneurons of the neostriatum. J Comp Neurol. 469(3):325–339.

Sullivan MA, Chen H, Morikawa H. 2008. Recurrent inhibitory network among striatal cholinergic interneurons. J Neurosci. 28(35):8682–8690.

Szydlowski SN, Pollak Dorocic I, Planert H, Carlen M, Meletis K, Silberberg G. 2013. Target selectivity of feedforward inhibition by striatal fast-spiking interneurons. J Neurosci. 33(4):1678–1683.

Tepper JM, Tecuapetla F, Koos T, Ibanez-Sandoval O. 2010. Heterogeneity and diversity of striatal GABAergic interneurons. Front Neuroanat. 4:150.

Threlfell S, Lalic T, Platt NJ, Jennings KA, Deisseroth K, Cragg SJ. 2012. Striatal dopamine release is triggered by synchronized activity in cholinergic interneurons. Neuron. 75(1):58–64.

Tricoire L, Pelkey KA, Erkkila BE, Jeffries BW, Yuan X, McBain CJ. 2011. A blueprint for the spatiotemporal origins of mouse hippocampal interneuron diversity. J Neurosci. 31(30):10948–10970.

Vuillet J, Kerkerian-Le Goff L, Kachidian P, Dusticier G, Bosler O, Nieoullon A. 1990. Striatal NPY-containing neurons receive GABAergic afferents and may also contain GABA: an electron microscopic study in the rat. Eur J Neurosci. 2(8):672–681.

Wirth MJ, Obst K, Wahle P. 1998. NT-4/5 and LIF, but not NT-3 and BDNF, promote NPY mRNA expression in cortical neurons in the absence of spontaneous bioelectrical activity. Eur J Neurosci. 10(4):1457–1464.

Xu Q, Tam M, Anderson SA. 2008. Fate mapping Nkx2.1-lineage cells in the mouse telencephalon. J Comp Neurol. 506(1):16–29.